RESEARCH ARTICLE
doi: 10.2306/scienceasia1513-1874.2026.007

ScienceAsia 51 (6): 2025: ID 2026007: **1–8**

Preparation and swelling performance of green algae polysaccharide-intelligent hydrogel

Dan Shi[a], **Xiaoying Lv**[b], **Xing Zhang**[c], **Ni Xie**[d], **Shasha Xu**[a], **Hongyi Qian**[a], **Yalin Li**[a,*]

[a] School of College of Environmental and Biological Engineering, Henan University of Engineering, Zhengzhou 451191 China
[b] Institute of Environmental Research at Greater Bay, Guangzhou University, Guangzhou 510006 China
[c] School of Civil Engineering, Architecture and Environment, Hubei University of Technology, Wuhan 430068 China
[d] School of Information Science and Technology, Hangzhou Normal University, Hangzhou 311121 China

*Corresponding author, e-mail: li_ya_lin@haue.edu.cn

Received 8 Jun 2025, Accepted 24 Dec 2025
Available online 15 Jan 2026

ABSTRACT: In recent years, the intensification of global climate change and the increased severity of water pollution have led to the explosive proliferation of microalgae, particularly Chlorophyta, significantly impacting the ecological environment. This study developed a novel adsorption hydrogel using extracellular polysaccharides (EPS) from green algae and acrylamide (AM) based on free-radical graft copolymerization technology, achieving the resource utilization of green algae. Using the swelling ratio (S_r) as the evaluation metric, the effects of the solid-to-liquid ratio, sodium persulfate (SPS), AM, N, N'-methylenebisacrylamide (MBA), and polymerization temperature on the hydrogel's swelling properties were systematically investigated. The optimal preparation conditions for the EPS/AM hydrogel were determined using response surface methodology, and the composition, structure, and morphology of the hydrogel were characterized using scanning electron microscopy. The results showed that the S_r of the green algae polysaccharide-based hydrogel reached its maximum of 35,541.34% under the following conditions: a solid-to-liquid ratio of 1:100, 0.1 g of SPS, 1.2 g of AM, 0.034 g of MBA, and a polymerization temperature of 80 °C. This study provides an innovative paradigm for the high-value utilization of functional polysaccharides, opening new pathways for the large-scale application of environmentally sensitive hydrogel materials through a closed-loop transformation model of "waste-to-functional materials".

KEYWORDS: green algae, swelling properties, hydrogel, response surface optimization

INTRODUCTION

The rapid industrialization of China has led to increasing scarcity of non-renewable resources (coal, oil, natural gas) and environmental challenges, spurring interest in renewable biomass resources [1]. Oceans, covering 71% of Earth's surface, offer vast potential for sustainable development [2]. Green algae (GA), abundant along China's coast [3], are often wasted due to inefficient treatment methods, resulting in the loss of valuable components (60% polysaccharides, 15–25% proteins) and the release of methane, which exacerbates the greenhouse effect [4].

Polysaccharides have become key biomaterials in medicine, food, and environmental engineering. GA contains $>60\%$ polysaccharides rich in functional groups (—OH, $-SO_4$, —COOH) with bioactive properties (antioxidant, immunomodulatory, antibacterial) [5]. Recent studies have further demonstrated the biomedical potential of plant-derived polysaccharides as bioactive compounds, such as their protective effects in disease-related models [6]. Their flexible chains, water solubility, and reactive sites enable molecular modifications and interactions [7], making them ideal for functional gels and high-value applications.

Hydrogels are 3D cross-linked networks of polymers and water, known for their excellent water absorption and retention [8, 9]. GA polysaccharides, with functional groups (—OH, —COOH, $-NH_2$), can form hydrogels through interactions like hydrogen bonding and electrostatic forces [10, 11]. Their biocompatibility enables diverse applications: Stan et al [12] developed Alg/PVA wound dressings with 264% swelling, while Ren et al [13] created UC-DPA-Ag hydrogels for diabetic wounds, achieving over 2,314% swelling. However, limited swelling performance hinders their application in wastewater treatment and controlled drug delivery [14]. Therefore, developing high-performance GA polysaccharide-based hydrogels with enhanced swelling capacity remains a key challenge for efficient utilization of algal resources.

In this study, extracellular polymeric substances (EPS) extracted from GA via microwave-alkaline treatment were polymerized into EPS-based intelligent hydrogels (EPSH) through free-radical copolymerization. Response surface methodology (RSM) was employed to optimize the swelling performance, and comprehensive characterization using SEM, FTIR, and XRD conducted to elucidate the structure-property relationship of the GA-EPS hydrogels.

MATERIALS AND METHODS

Materials

Sodium hydroxide (NaOH, $\geqslant 96\%$), acrylamide (monomer, AM, 99%), N, N'-methylenebisacrylamide

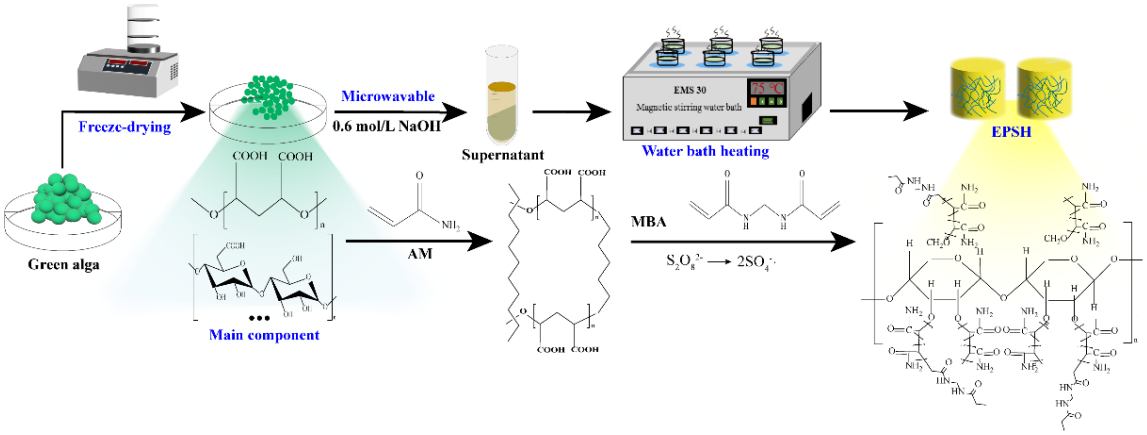

Fig. 1 Basic principle and process of hydrogel preparation.

(crosslinking agent, MBA, 99%), sodium persulfate (initiator, SPS, 99%), and anhydrous ethanol (C_2H_6O, 98%) were purchased from Shanghai Aladdin Biochemical Technology Co., Ltd., Shanghai, China. All reagents were of analytical grade and used without further purification. Deionized water was used throughout the experiments.

Preparation of EPSH

GA-EPS was extracted using microwave-assisted alkaline treatment [15, 16]: 1.0 g algal powder in 100 ml 0.6 M NaOH, microwaved (560 W, 20 s; Midea EM7KCGW3-NR), then centrifuged (4,000 rpm, 15 min) to obtain EPS. EPSH was synthesized via radical graft copolymerization [17]: EPS was dispersed (75 °C, 15 min; HSJ water bath), followed by sequential addition of AM (10 min reaction), MBA (5 min), and SPS. After 1 min reaction, the mixture was formed using residual heat, then washed three times. The synthesis route is shown in Fig. 1.

Determination of swelling property of EPSH

Using the most common tea bag method to determine the swelling rate of hydrogels [18], the experimental accuracy can reach 3.5%. The swelling performance of EPSH was evaluated using Eq. (1) [19].

$$S_r = \frac{W_e - W_d}{W_d} \times 100\% \quad (1)$$

where W_e and W_d are the mass (g) of dry hydrogel and hydrogel after swelling equilibrium, respectively, S_r is the maximum swelling rate of hydrogel (%).

Single factor experimental design

In this study, EPS solution was extracted from GA using a microwave-assisted alkaline method. C@EPSs and NaOH with varying material-to-liquid ratios were used as the solution carrier. AM was used as the monomer, SPS as the initiator, and MBA as the crosslinker, with different reaction temperatures (T). In each single-factor experiment, only one variable was changed, while the remaining synthesis conditions were kept at their optimal baseline values to ensure comparability of results. The synthesis conditions of EPSH were first optimized by single factor experiments (SFE), followed by response surface optimization to develop a high-swelling hydrogel, achieving the value-added utilization of GA. The SFE factors are shown in Table S1.

Optimizing experimental design

Based on the SFE, the data were analyzed using Design Expert 13.0 software to eliminate interactions between factors. Variance analysis assessed model performance and statistical validation, with response surfaces and contour plots visualizing factor interactions. Coefficient significance was determined by p-values and F-values. The independent variables for optimization are material-liquid ratio (A), AM amount (B), and MBA amount (C), with S_r as the response. Factor coding levels are shown in Table S2.

Characterization of raw materials and hydrogel morphology

The morphology of GA and hydrogels was characterized using SEM (Zeiss Sigma 300). Samples were prepared by freeze-drying GA and swelling hydrogels to equilibrium in deionized water before freeze-drying (LGJ-100, 24 h) to preserve pore structure [20]. Samples were gold-sputtered prior to SEM imaging to analyze surface morphology and internal porosity. FTIR spectra were recorded using an IRTracer-100 spectrometer (Shimadzu, Japan) over the range of 4,000–500 cm^{-1} with a resolution of 4 cm^{-1}. XRD patterns were collected on a D8 ADVANCE diffractometer (Bruker, Germany) using Cu Kα radiation (λ = 1.5406 Å) over a 2θ range of 5–80° with a step size of 0.02° and a scanning rate of 2°/min.

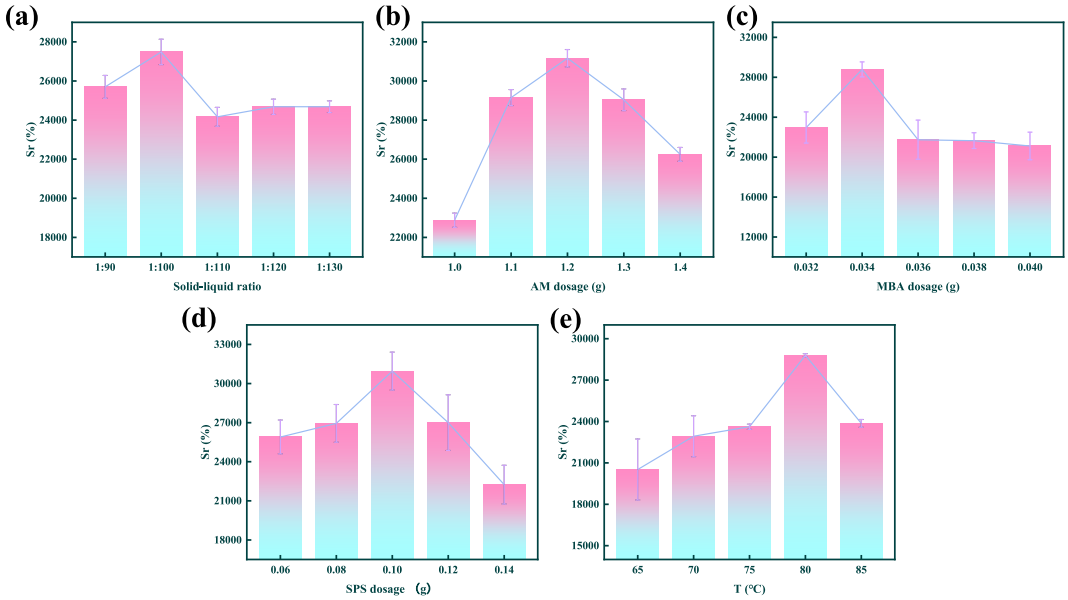

Fig. 2 Effect of (a) solid-liquid radio, (b) AM dosage, (c) MBA dosage, (d) SPS dosage, and (d) temperature on hydrogel swelling rate.

RESULTS AND DISCUSSION

Effect of material-liquid ratio

An appropriate solid-to-liquid ratio promotes thorough interaction between GA and the extraction solution; ratios that are too high or too low will reduce polysaccharide extraction rates. This ratio is a key factor influencing EPSH swelling capacity. In this section, experiments were conducted using five different solid-to-liquid ratios (1:90, 1:100, 1:110, 1:120, 1:130), while other parameters were maintained at constant levels. Specifically, the AM dosage was 1.3 g, SPS dosage was 0.10 g, polymerization temperature was 75 °C, and MBA dosage was set to 0.04 g [21]. Fig. 2(a) shows that the solid-liquid ratio influences polysaccharide dissolution and hydrogel swelling through hydrophilic interactions between EPS functional groups (−OH/−COOH) and water [22]. The optimal 1:100 ratio achieved maximum swelling (27,385.08%), balancing polysaccharide content and network porosity. Higher ratios caused network densification that limited water diffusion despite increased hydrophilicity, leading to swelling saturation [23]. Thus, 1:100 was selected as optimal.

Effect of AM dosage

AM forms a covalent crosslinked network structure under the initiation of SPS, which is a key factor influencing the swelling properties of EPSH. In this section, experiments were conducted at five equal gradient AM dosages (1.00 g, 1.10 g, 1.20 g, 1.30 g, 1.40 g), with all other parameters held constant. Specifically, the solid-to-liquid ratio was 1:100, SPS dosage was 0.10 g, polymerization temperature was 75 °C, and MBA dosage was set to 0.04 g. As shown in Fig. 2(b), at low AM concentrations, the limited incorporation of AM monomers into the polymer matrix leads to a loosely crosslinked network with high porosity, which facilitates water uptake and enhances the swelling capacity [24]. In contrast, when the AM dosage exceeds 1.20 g, the increased availability of AM chains between MBA crosslinking points effectively elevates the overall network density and reduces the free volume, resulting in a more compact structure that restricts water diffusion [25]. The reduced free volume also impairs water retention, ultimately decreasing swelling performance. Therefore, 1.20 g AM was selected as the optimal condition.

Effect of MBA dosage

The dosage of crosslinking agent MBA is a key factor influencing hydrogel crosslinking density and effective chemical crosslinking points. In this section, experiments were conducted at five equal-gradient MBA dosages (0.032 g, 0.034 g, 0.036 g, 0.038 g, 0.040 g), while all other parameters were maintained at constant levels. Specifically, the feed solution ratio was 1:100, the SPS dosage was 0.10 g, the polymerization temperature was 75 °C, and the AM dosage was set to 1.20 g. MBA serves as both a crosslinker and a participant in intermolecular interactions with AM, influencing hydrogel swelling by modulating crosslinking density. Fig. 2(c) shows hydrogel swelling initially increased then decreased with MBA content, peaking at 28,270.05% (0.034 g MBA). Optimal crosslinking is crucial for 3D network formation – insufficient MBA

yields weak structures [26], while excess creates rigid networks that hinder water absorption [27]. Thus, 0.034 g MBA was selected as the optimal condition.

Effect of SPS dosage

SPS serves as an initiator in hydrogel synthesis, with its core function being the generation of sulfate radicals through pyrolysis, thereby triggering the radical polymerization of AM monomers. In this section, experiments were conducted at five equal-gradient SPS dosages (0.06 g, 0.08 g, 0.10 g, 0.12 g, 0.14 g), with all other parameters held constant. Specifically, the feedstock-to-solvent ratio was 1:100, the MBA dosage was 0.034 g, the polymerization temperature was 75 °C, and the AM dosage was set to 1.20 g. SPS free radicals initiate polymerization with AM and MBA, forming varying polymer chain lengths that influence the hydrogel's 3D network stability and water absorption. Fig. 2(d) shows the swelling rate initially increased with SPS amount, peaking at 30,953.84% (0.10 g SPS), then decreased at higher dosages. At low SPS dosages, insufficient free radicals reduce monomer conversion and hinder chain initiation [28]. Increasing SPS boosts $2\,SO_4^{-\bullet}$ radicals, enhancing AM-EPS polymerization and AM self-polymerization by generating more hydroxyl radicals on EPS chains. However, excess SPS accelerates $2\,SO_4^{-\bullet}$ and $S_2O_8^{2-\bullet}$ decomposition (Eq. (2)), causing rapid radical quenching [29]. This surge in active centers accelerates chain termination, shortening polymer chains and reducing hydrogel molecular weight, ultimately diminishing swelling performance.

$$S_2O_8^{2-} \rightarrow 2\,SO_4^{-\bullet} \tag{2}$$

Effect of temperature

Temperature plays a crucial regulatory role in the swelling properties of hydrogels. In this section, experiments were conducted at five equal-gradient polymerization temperatures (65 °C, 70 °C, 75 °C, 80 °C, 85 °C), with all other parameters maintained at constant levels. Specifically, the feed ratio was set at 1:100, with 0.034 g of MBA, 0.10 g of SPS, and 1.20 g of AM. EPSH forms a 3D network through crosslinking polymerization under heat, and reaction temperature may affect its swelling properties. Fig. 2(e) shows that higher temperatures accelerate molecular thermal motion and radical collisions, affecting water molecule diffusion in hydrogels. At low temperatures, slower diffusion allows stable hydrogen bonds between water and hydrophilic groups, enhancing water absorption [30]. Above 80 °C, faster diffusion increases water loss, reducing absorption capacity. Although high temperature speeds up water movement, hydrogel swelling is limited by high crosslinking density and poor water retention [31]. Additionally, elevated temperatures may degrade functional groups, particularly temperature-sensitive hydrophilic groups in GA-EPS, further impairing swelling performance.

RSM analysis

The central composite design of design expert was used to optimize the optimal conditions for hydrogel preparation. The material-liquid ratio (a), AM (b) and MBA (c) were selected as the investigation factors. The factor design level of the experiment is shown in Table S2. The second-order model analysis method was used to analyze and fit the data according to the regression equation, and the quadratic regression surface equation was established. The surface equation is shown in Eq. (3).

$$\begin{aligned} S_r = &-1.81\times10^6+1.08\times10^4\times A+1.06\times10^6\times B+3.98\times10^7\times C \\ &-25.99\times A\times B-7.23\times10^4\times A\times C-5.45\times10^6 \\ &-41.78\times A^2-3.63\times10^5\times B^2-3.89\times10^8\times C^2 \end{aligned} \tag{3}$$

The analysis of variance (Table 1) shows that $F = 45.28$, $p \leqslant 0.05$, with a mismatch p value of 0.6347 (> 0.05), indicating significant model fitting. The determination coefficient $R^2 = 0.9831$, adjusted $R^2 = 0.9614$, and variation coefficient = 2.21%, significantly lower than 10%. The signal-to-noise ratio of 16.42, greater than 4, confirms high experimental accuracy and feasibility, with small prediction errors. The effects of solid-liquid ratio, AM dosage, and MBA dosage on S_r are well simulated.

Fig. 3 shows maximum S_r occurs near optimal factor values, confirming prediction accuracy and significant factor interactions. Analysis reveals that adjusting liquid-solid ratio, AM, and MBA content effectively enhances EPSH swelling (Fig. 3(a,b)). Optimization experiments (Fig. 3(c–f)) identified ideal conditions: 1:100 liquid-solid ratio, 1.204 g AM, and 0.034 g MBA, achieving peak S_r of 35,541.34%. Verification tests showed $< 10\%$ error between predicted and actual S_r values, validating the model's accuracy.

To evaluate the accuracy and deviation of the optimized experimental data, three groups of experiments were randomly selected for verification, as shown in Table 2. This Table demonstrates that the predicted values of the three experimental models align well with the actual values, with relative errors less than 10%, indicating the model's high reliability and suitability for high experimental accuracy.

Characterization

SEM analysis

To explore the mechanism of hydrogel with high swelling property, the GA and EPSH samples were characterized by SEM, and the results are shown in Fig. 4. GA shows a compact, low-porosity structure with no visible pores (Fig. 4(a,b)) [33]. In contrast, freeze-dried EPSH exhibits a porous 3D network (Fig. 4(c,d)), formed through crosslinking of GA polysaccharide functional groups. This structure provides water storage space and facilitates rapid water penetration [34], while hydroxyl/carboxyl groups on pore walls maintain structural stability through hydrogen bonding with water molecules.

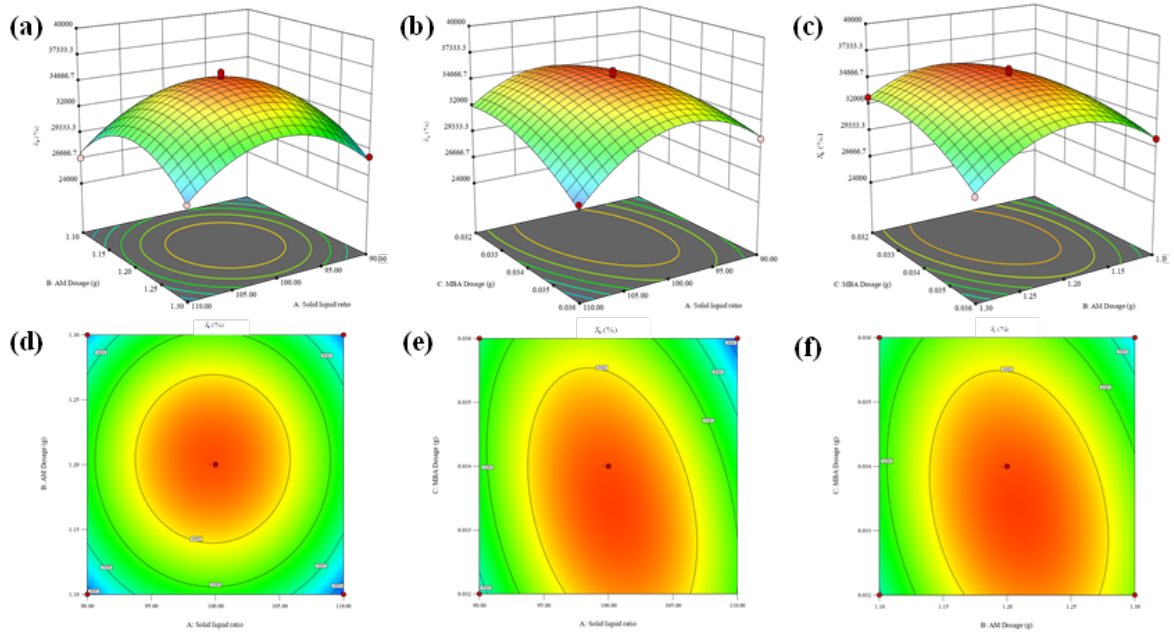

Fig. 3 Three-dimensional response surface and contour plots: (a), (d) AM content and liquid-to-solid ratio; (b), (e) MBA content and liquid-to-solid ratio; (c), (f) AM and MBA content.

Table 1 Analysis of variance of the equation.

Source	Sum of variance squares	Degree of freedom	Variance	F-value	Prob > F	Significance
Model	1.89×10^8	9	2.10×10^8	45.28	< 0.0001	Significant
A	2.18×10^5	1	2.18×10^5	0.4703	0.5149	
B	8.59×10^5	1	8.59×10^5	1.85	0.2154	
C	5.93×10^6	1	5.93×10^6	12.79	0.0090	
AB	2,887.29	1	2,887.29	0.0062	0.9393	
AC	6.86×10^6	1	6.86×10^6	14.80	0.0063	
BC	5.08×10^6	1	5.08×10^6	10.96	0.0129	
A2	6.87×10^7	1	6.87×10^7	148.40	< 0.0001	
B2	4.55×10^7	1	4.55×10^7	98.11	< 0.0001	
C2	9.55×10^6	1	9.55×10^6	20.61	0.0027	
Residual	3.24×10^6	7	4.63×10^5			
Anomalistic term	1.04×10^6	3	3.46×10^5	0.6268	0.6347	Not significant
Pure error	2.21×10^6	4	5.51×10^5			
Total deviation	1.92×10^8	16				

FTIR analysis

To investigate whether crosslinking occurred in the hydrogel, FTIR analysis was performed on GA-EPS and the resulting EPSH, with the results shown in Fig. 5. The raw material GA-EPS exhibits characteristic peaks at 1,560, 1,395, and 1,312 cm^{-1} corresponding to —NH bending vibrations (amide II band), —COO^- symmetric stretching, C—H bending, and C—N/C— stretching vibrations, respectively [35, 36]. However, compared to GA-EPS, the intensities of these absorption peaks in EPSH were significantly weakened, and some peak positions shifted slightly, indicating that these functional groups underwent chemical changes

Table 2 Validation of experimental data.

Serial no.	Material-liquid ratio	AM dosage (g)	MBA dosage (g)	S_r measured value (%)	S_r predicted value (%)	Inaccuracy
1	1:100	1.10	0.036	31,104.91	30,194.01	−3.02
2	1:100	1.30	0.036	29,993.84	28,658.21	−4.66
3	1:90	1.20	0.032	31,113.52	29,418.52	−5.76

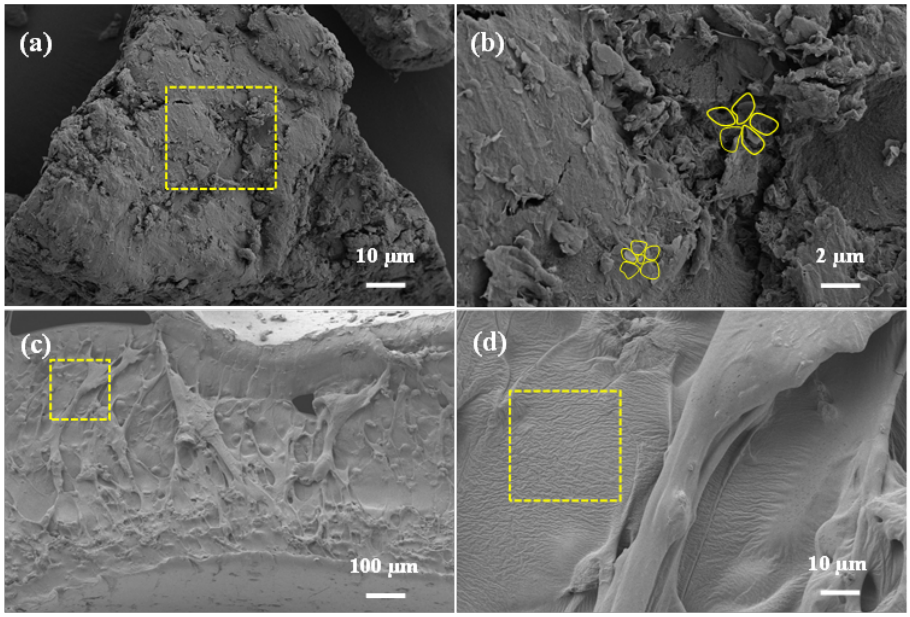

Fig. 4 SEM images: (a) and (b) GA; (c) and (d) EPSH hydrogel.

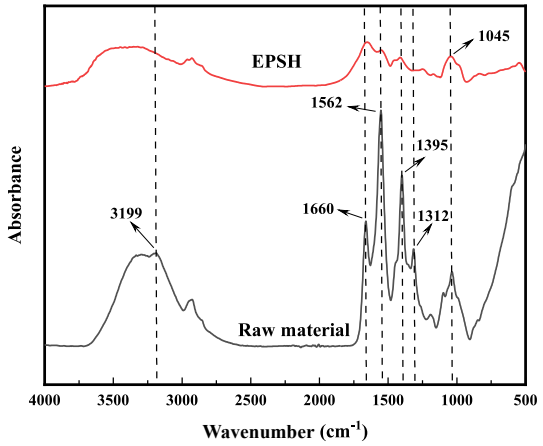

Fig. 5 FTIR spectra of GA-EPS and EPSH.

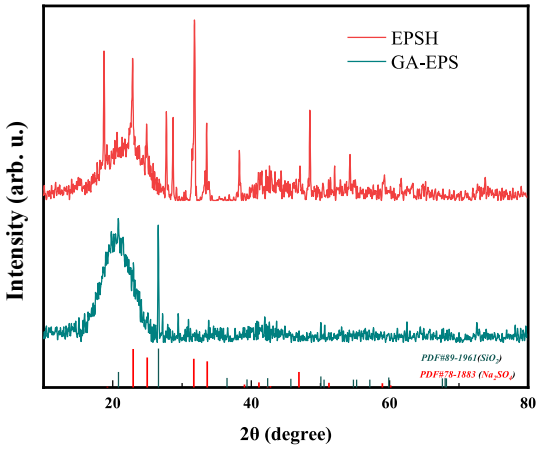

Fig. 6 XRD pattern of GA-EPS and EPSH.

during the polymerization reaction. Specifically, the reduction in the 1560 cm^{-1} peak indicates that —NH or —COO^- groups participated in cross-linking reactions with acrylamide.

The attenuation of the 1,395 and 1,312 cm^{-1} peaks suggests altered chemical environments for C—N, C—O, and —OH groups, potentially forming new amide bonds or hydrogen bond networks. Concurrently, the persistence of the C—O—C stretching vibration peak at 1045 cm^{-1} indicates that the polysaccharide backbone structure remains largely intact [37]. Collectively, the overall weakening and shift of characteristic peaks in EPSH conclusively demonstrate that the active functional groups in GA-EPS have participated in radical grafting and cross-linking reactions, thereby constructing a stable three-dimensional network structure [38].

XRD analysis

As shown in Fig. 6, GA-EPS exhibits a broad, low-intensity peak at $2\theta \approx 20°$, indicating an overall amorphous structure [39]. Additionally, the signal corresponding to the 26.62° peak aligns with the SiO_2 diffraction position in the PDF#89-1961 standard card, suggesting this diffraction peak primarily originates from naturally occurring minerals within the algal body or residual silica from the extraction process [40]. In contrast, the EPSH sample exhibits several distinct diffraction peaks at $2\theta \approx 22.85°$, 31.90°, and 48.47°, which show good agreement with the PDF#78-1883

(Na_2SO_4) standard card. This indicates these peaks originate from Na_2SO_4 crystals, a byproduct formed during the decomposition of SPS in the polymerization reaction [41]. Given the hydrogel matrix's highly crosslinked amorphous network structure, these sharp peaks result not from polymer crystallization but from precipitated residual inorganic salts. This further confirms that SPS decomposed during initiation, releasing free radicals that participated in the grafting reaction between EPS and AM.

Combined with the FTIR analysis showing weakened absorption peaks for functional groups such as —NH, —OH, and —COOH, it can be inferred that the formation of EPSH involves chemical cross-linking and structural rearrangement. GA-EPS has been successfully transformed from a natural amorphous polysaccharide into a hydrogel material with a functionalized network structure.

CONCLUSION

In this study, GA polysaccharides were extracted by a microwave-assisted alkaline method and polymerized into high-swelling hydrogels. The effects of key preparation parameters on swelling behavior were investigated, and the optimal conditions were determined using RSM, under which a maximum swelling ratio of 35,541.34% was achieved. Statistical analysis showed that the swelling performance was mainly affected by MBA dosage, followed by AM dosage and material-to-liquid ratio. SEM revealed a porous interconnected network structure, while FTIR and XRD analyses confirmed the successful formation of a cross-linked hydrogel with a predominantly amorphous structure. These results indicate that GA polysaccharides are promising renewable resources for high-swelling hydrogel preparation. Future work will focus on improving mechanical properties while maintaining high swelling performance.

Appendix A. Supplementary data

Supplementary data associated with this article can be found at https://dx.doi.org/10.2306/scienceasia1513-1874.2026.007.

Acknowledgements: This study was supported by the Science and Technology Tack ling Projects in Henan Province in 2025 (No. 252102321172).

REFERENCES

1. Saldarriaga HS, Hernandez VG, Iqbal HMN, Barceló D, Parra SR (2020) Bioremediation potential of *Sargassum* sp. biomass to tackle pollution in coastal ecosystems: Circular economy approach. *Sci Total Environ* **715**, 136978.
2. Yan M, Jiang S (2023) Recent trends in functional characteristics and degradation methods of alginate. *Bio Web Conf* **61**, 01015.
3. Phanprasert Y, Maciszewski K, Gentekaki E, Dacks JB (2023) Comparative genomic analysis illustrates evolutionary dynamics of multisubunit tethering complexes across green algal diversity. *J Environ Manage* **70**, e12935.
4. Zabochnicka M, Krzywonos M, Romanowska DZ, Szufa S, Darkalt A, Mubashar M (2022) Algal biomass utilization toward circular economy. *Life* **12**, 1480.
5. Chaisuwan W, Phimolsiripol Y, Chaiyaso T, Techapun C, Leksawasdi N, Jantanasakulwong K, Seesuriyachan P (2021) The antiviral activity of bacterial, fungal, and algal polysaccharides as bioactive ingredients: potential uses for enhancing immune systems and preventing viruses. *Front Nutr* **8**, 772033.
6. Lin C, Lu H (2024) Protective effect and mechanisms of *Chimonanthus salicifolius* polysaccharide on acute alcoholic liver injury in mice. *ScienceAsia* **50**, ID 2024112.
7. Beaumont M, Tran R, Vera G, Niedrist D, Rousset A, Pierre R, Forget A (2021) Hydrogel-forming algae polysaccharides: From seaweed to biomedical applications. *Biomacromolecules* **22**, 1027–1052.
8. Sun R, Gao S, Zhang K, Cheng W, Hu G (2024) Recent advances in alginate-based composite gel spheres for removal of heavy metals. *Int J Biol Macromol* **268**, 131853.
9. Zhu T, Ni Y, Biesold GM, Cheng Y, Ge M, Li H, Lai Y (2023) Recent advances in conductive hydrogels: classifications, properties, and applications. *Chem Soc Rev* **52**, 473.
10. Manzoor A, Dar AH, Pandey VK, Shams R, Khan S, Panesar PS, Khan SA (2022) Recent insights into polysaccharide-based hydrogels and their potential applications in food sector: A review. *Int J Biol Macromol* **213**, 987–1006.
11. Gieroba B, Kalisz G, Krysa M, Khalavka M, Przekora A (2023) Application of vibrational spectroscopic techniques in the study of the natural polysaccharides and their cross-linking process. *Int J Mol Sci* **24**, 2630.
12. Stan D, Mirica AC, Mocanu S, Stan D, Podolean I, Candu N, Coman SM (2025) Hybrid hydrogel supplemented with algal polysaccharide for potential use in biomedical applications. *Gels* **11**, 17.
13. Ren Y, Aierken A, Zhao L, Lin Z, Jiang J, Li B, Tu Q (2022) hUC-MSCs lyophilized powder loaded polysaccharide ulvan driven functional hydrogel for chronic diabetic wound healing. *Carbohydr Polym* **288**, 119404.
14. Ghiorghita CA, Dinu MV, Lazar MM, Dragan E (2022) Polysaccharide-based composite hydrogels as sustainable materials for removal of pollutants from wastewater. *Molecules* **27**, 8574.
15. Zhang Y, Lei Y, Qi S, Fan MX, Zheng S, Huang QB, Lu X (2023) Ultrasonic-microwave-assisted extraction for enhancing antioxidant activity of *Dictyophora indusiata* polysaccharides: The difference mechanisms between single and combined assisted extraction. *Ultrason Sonochem* **95**, 106356.
16. Qin L, Yang Y, Mao W (2023) Anticoagulant property of a sulfated polysaccharide with unique structural characteristics from the green alga *Chaetomorpha aerea*. *Mar Drugs* **21**, 88.
17. Patel P, Thareja P (2022) Hydrogels differentiated by length scales: A review of biopolymer-based hydrogel preparation methods, characterization techniques, and targeted applications. *Eur Polym J* **163**, 110935.

18. Feroze F, Sher M, Hussain MA, Abbas A, Haseeb MT, Fatima A, Amin HM (2025) Gastro retentive floating drug delivery system of levofloxacin based on *Aloe vera* hydrogel: *In vitro* and *in vivo* assays. *Int J Biol Macromol* **284**, 138156.
19. Abdel-Hakim A, El-Gamal AA, El-Zayat MM, Sadek AM (2021) Effect of novel sunrose based polyfunctional electrical properties of irradiated EPDM. *Rad Phys Chem* **189**, 109729.
20. Odziomek K, Drabczyk AK, Kościelniak P, Konieczny P, Barczewski M, Bialik-Was K (2024) The role of freeze-drying as a multifunctional process in improving the properties of hydrogels for medical use. *Pharmaceutics* **17**, 1512.
21. Levy-Ontman O, Yanay C, Paz-Tal O, Wolfson A (2023) Red algae sulfur-based polysaccharides as bioadsorbents for europium removal from aqueous solutions. *J Polym Environ* **31**, 2321.
22. Concórdio RP, Martins M, Araújo D, Alves VD, Moppert X, Guézennec J, Freitas F (2024) Iron (III) cross-linked hydrogels based on *Alteromonas macleodii* Mo 169 exopolysaccharide. *Int J Biol Macromol* **274**, 133312.
23. Ma X, Duan D, Chen J, Xie B (2022) Structure and adsorption performance of cationic *Entermorpha prolifera* polysaccharide-based hydrogel for typical pollutants: Methylene blue, cefuroxime, and Cr (VI). *Gels* **8**, 546.
24. El IA, El GA, Achagri G, Essamlali Y, Amadine O, Akil A, Zahouily M (2022) Synthesis of urea-containing sodium alginate-g-poly (acrylic acid-co-acrylamide) superabsorbent-fertilizer hydrogel reinforced with carboxylated cellulose nanocrystals for efficient water and nitrogen utilization. *J Environ Chem Eng* **10**, 108282.
25. Feng W, Wang Z (2023) Tailoring the swelling-shrinkable behavior of hydrogels for biomedical applications. *Sci Adv* **10**, 2303326.
26. Li Y, Huang Y, Liu L, Liu H, He H, Lu D, Dong T (2023) Nano-CaO_2 promotes the release of carbon sources from municipal sludge and the preparation of double-network hydrogels with high swelling ratios. *Renewable Mater* **11**, 1237–1253.
27. Kędziersk M, Jamroży M, Drabczyk A, Kudłacik K S, Bńkosz M, Gruca M, Tyliszczak B (2022) Analysis of the influence of both the average molecular weight and the content of crosslinking agent on physicochemical properties of PVP-based hydrogels developed as innovative dressings. *Int J Mol Sci* **23**, 11618.
28. Huang Y, Zhang X, Shi D, Qian H, Zhao J, Xu S, Li Y (2025) Orthogonal test optimization of swelling performance in kitchen waste carbon source hydrogels. *Processes* **13**, 110.
29. Li Y, Liu L, Zhang X, Dong T, Wang Z, Xiong M, Zhao J (2024) Investigating the mechanical properties of hydrogels prepared from food waste: A study based on molecular dynamics simulations. *Waste Bio Valor* **16**, 2167–2184.
30. Wang H, Lu Z, Wang F, Li Y, Qu Z, Jiang J (2023) A novel strategy to reinforce double network hydrogels with enhanced mechanical strength and swelling ratio by nano cement hydrates. *Polymer* **269**, 125725.
31. Balan KE, Boztepe C, Künkül A (2022) Modeling the effect of physical crosslinking degree of pH and temperature responsive poly (NIPAAm-co-VSA)/alginate IPN hydrogels on drug release behavior. *J Drug Deliv Sci Tec* **75**, 103671.
32. Meng X, Ye D, Pan Y, Zhang T, Liang L, Liu L, Ma Y (2024) Optimisation of not-from-concentrate goji juice processing using fuzzy mathematics and response surface methodology and its quality assessment. *Appl Sci* **14**, 8393.
33. Zha F, Huang K, Kang B, Sun X, Su J, Li Y, Lu Z (2022) Deterioration characteristic and constitutive model of red-bed argillaceous siltstone subjected to drying-wetting cycles. *Lithosphere* **1**, 8786210.
34. Griveau L, Lafont M, Le GH, Drouglazet C, Robbiani B, Berthier A, Sohier J (2022) Design and characterization of an *in vivo* injectable hydrogel with effervescently generated porosity for regenerative medicine applications. *Acta Biomater* **140**, 324.
35. Sadat A, Joye IJ (2020) Peak fitting applied to Fourier transform infrared and Raman spectroscopic analysis of proteins. *Appl Sci* **10**, 5918.
36. Mitra S, Werling K, Berquist EJ, Lambrecht DS, Garrett RS (2021) CH mode mixing determines the band shape of the carboxylate symmetric stretch in Apo-EDTA, Ca^{2+}-EDTA, and Mg^{2+}-EDTA. *J Phys Chem A* **125**, 4867–4881.
37. Gieroba B, Kalisz G, Krysa M, Khalavka M, Przekora A (2023) Application of vibrational spectroscopic techniques in the study of the natural polysaccharides and their cross-linking process. *Int J Mol Sci* **24**, 2630.
38. Pragya A, Mutalik S, Younas MW, Pang SK, So PK, Wang F, Zheng Z, Noor N (2021) Dynamic cross-linking of an alginate-acrylamide tough hydrogel system: time-resolved *in situ* mapping of gel self-assembly. *RSC Adv* **11**, 10710–10726.
39. Jatoi SM, Rehman S, Abbas K, Liang R, Peng J (2023) Hydroxyethyl cellulose-based hydrogels as controlled-release carriers. *Molecules* **28**, 7320.
40. Germinario L, Oguchi CT (2022) Gypsum, mirabilite, and thenardite efflorescences of tuff stone in the underground environment. *Environ Earth Sci* **81**, 772.
41. Zhang H, Wang W, Ma J (2020) Research on the mechanism and reaction conditions of electrochemical activation of peroxydisulfate: sulfate-radical generation pathways. *RSC Adv* **10**, 29047–29058.

Appendix A. Supplementary data

Table S1 SFE experimental factors and levels.

Parameter	Unit	Level				
		1	2	3	4	5
Material-liquid ratio		1:90	1:100	1:110	1:120	1:130
AM dosage	g	1.00	1.10	1.200	1.300	1.400
SPS dosage	g	0.06	0.08	0.100	0.120	0.140
MBA dosage	g	0.032	0.034	0.036	0.038	0.040
Temperature (T)	℃	65.00	70.00	75.00	80.00	85.00

Table S2 Boundary conditions of independent variables in response optimization.

Variable	Unit	Coding level		
		−1	0	+1
A: Material-liquid ratio	g/ml	1:100	1:90	1:110
B: AM dosage	g	1.100	1.200	1.300
C: MBA dosage	g	0.032	0.034	0.036